

TOPICAL REVIEW

## Study of van der Waals bonding and interactions in metal organic framework materials

To cite this article: Sebastian Zuluaga *et al* 2014 *J. Phys.: Condens. Matter* **26** 133002

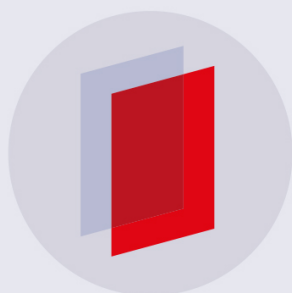
View the [article online](#) for updates and enhancements.

### Related content

- [Spectroscopic characterization of van der Waals interactions in a metal organic framework with unsaturated metal centers: MOF-74–Mg](#)  
Nour Nijem, Pieremanuele Canepa, Lingzhu Kong *et al.*
- [Computational materials chemistry for carbon capture using porous materials](#)  
Abhishek Sharma, Runhong Huang, Ateeque Malani *et al.*
- [van der Waals forces in density functional theory: a review of the vdW-DF method](#)  
Kristian Berland, Valentino R Cooper, Kyuho Lee *et al.*

### Recent citations

- [Antonio Romerosa and Franco Scalambra](#)
- [Computational Design of Functionalized Imidazolate Linkers of Zeolitic Imidazolate Frameworks for Enhanced CO<sub>2</sub> Adsorption](#)  
M. Althaf Hussain *et al*
- [van der Waals forces in density functional theory: a review of the vdW-DF method](#)  
Kristian Berland *et al*



**IOP | ebooks™**

Bringing you innovative digital publishing with leading voices to create your essential collection of books in STEM research.

Start exploring the collection - download the first chapter of every title for free.

## Topical Review

# Study of van der Waals bonding and interactions in metal organic framework materials

Sebastian Zuluaga<sup>1</sup>, Pieremanuele Canepa<sup>1</sup>, Kui Tan<sup>2</sup>, Yves J Chabal<sup>2</sup> and Timo Thonhauser<sup>1</sup>

<sup>1</sup> Department of Physics, Wake Forest University, Winston-Salem, NC 27109, USA

<sup>2</sup> Department of Materials Science and Engineering, University of Texas at Dallas, TX 75080, USA

E-mail: [thonhauser@wfu.edu](mailto:thonhauser@wfu.edu)

Received 12 December 2013, revised 22 January 2014

Accepted for publication 24 January 2014

Published 11 March 2014

## Abstract

Metal organic framework (MOF) materials have attracted a lot of attention due to their numerous applications in fields such as hydrogen storage, carbon capture and gas sequestration. In all these applications, van der Waals forces dominate the interaction between the small guest molecules and the walls of the MOFs. In this review article, we describe how a combined theoretical and experimental approach can successfully be used to study those weak interactions and elucidate the adsorption mechanisms important for various applications. On the theory side, we show that, while standard density functional theory is not capable of correctly describing van der Waals interactions, functionals especially designed to include van der Waals forces exist, yielding results in remarkable agreement with experiment. From the experimental point of view, we show examples in which IR adsorption and Raman spectroscopy are essential to study molecule/MOF interactions. Importantly, we emphasize throughout this review that a combination of theory and experiment is crucial to effectively gain further understanding. In particular, we review such combined studies for the adsorption mechanism of small molecules in MOFs, the chemical stability of MOFs under humid conditions, water cluster formation inside MOFs, and the diffusion of small molecules into MOFs. The understanding of these phenomena is critical for the rational design of new MOFs with desired properties.

Keywords: metal organic frameworks, van der Waals, vdW-DF, IR adsorption and Raman spectroscopy

(Some figures may appear in colour only in the online journal)

## Contents

1. Introduction	2	2.2. Difficulty of IR and Raman spectroscopy to describe small molecule adsorption in MOFs	3
2. Success and failure of vibrational spectroscopies to study van der Waals interactions	2	2.3. Experimentation	3
2.1. IR and Raman spectroscopy of small molecule adsorption in MOFs	2	3. Computer simulations as a tool to interpret complex spectroscopic experiments	4
		3.1. <i>Ab initio</i> modeling of materials	4

3.2. vdW-DF: a good compromise between cost and accuracy	4
3.3. Comparison between vdW-DF simulations and experiment	5
4. Examples of successful combined experimental/theoretical studies	5
4.1. Studying adsorption mechanisms of small molecules in MOFs	5
4.2. Studying the chemical stability of MOFs under humid conditions	6
4.3. Studying the formation of water clusters in fluorinated MOFs	8
4.4. Studying small molecule diffusion in MOFs	9
5. Summary and outlook	11
Acknowledgment	11
References	11

## 1. Introduction

Metal organic framework (MOF) materials are nano-porous materials comprised of metal centers, which are linked by organic ligands. Over the past decade, MOFs have attracted a surge of attention due to their extraordinary properties, useful for hydrogen storage [1–4], CO<sub>2</sub> capture [5–9], catalysis [10–12] and sensing [13] among others [14, 15]. Part of the success of MOFs also has to do with their often simple synthesis, i.e. by combining the organic ligands and the metallic salt in a solvothermal reaction [16, 17]. Most practical applications of MOFs rely on a specific interaction of the MOF with small molecules. This interaction—typically of a weak van der Waals type—has thus been at the center of many experimental and theoretical studies. It is exactly the understanding of this interaction that will allow us to interpret the properties of current MOFs better, and design new and improved MOFs with desired properties. For example, we do know that, in general, the surface area of the MOFs and the binding strength to the metal centers are the two main factors controlling the uptake of small molecules. However, the exact correlation between those properties is unclear [18]. Another example that concerns much current research, is trying to address the problem of low stability of MOFs under humid conditions. While some progress has been made [19–24], the newly found water-resistant MOFs often lack the desired specific molecular uptakes that are needed. Overall, progress has been slow to address such questions due to a lack of appropriate methods to study the molecular interactions inside MOFs. In the present review article we highlight a strategy, combining experiment and theory, that overcomes these problems and has been particularly successful in unraveling van der Waals interactions in MOFs.

The experimental study of those interactions often relies on powerful vibrational spectroscopy such as infrared (IR) absorption and Raman scattering, which indirectly provide information about the molecular adsorption process taking place in the MOF. The theoretical description with *ab initio* methods, due to the typical size of MOF unit cells

and their extended nature, rules out most highly accurate quantum-chemistry approaches and leaves density functional theory (DFT) as the only viable option. Historically, however, standard exchange–correlation functionals within DFT such as the local density approximation (LDA) and the generalized gradient approximation (GGA) only poorly capture van der Waals interactions. We will show here that the specially designed functional vdW-DF [25–27] is in fact capable of describing van der Waals interactions reliably and gives results in remarkable agreement with experiment.

This review article aims to showcase the importance of IR and Raman spectroscopy techniques combined with *ab initio* simulations at the DFT level (utilizing vdW-DF) as a promising way to study and rationally design complex systems where van der Waals bonding plays a major role. To this end, this work is divided into several sections. In section 2, we give a description of the successes and failures of vibrational spectroscopic techniques to study van der Waals interactions. Then, in section 3, we present a description of the computer simulations used to describe and interpret complex spectroscopic experiments. In section 4, we present several relevant examples where the combination of experiment and theory explains the behavior of various MOF systems and provides much needed understanding. We conclude with a short summary and outlook in section 5.

## 2. Success and failure of vibrational spectroscopies to study van der Waals interactions

### 2.1. IR and Raman spectroscopy of small molecule adsorption in MOFs

IR and Raman spectroscopy provide complementary information about bonding configurations through their vibrational spectra. IR spectra reflect photon absorption during transitions from ground to first-excited vibrational levels ( $\nu = 0 \rightarrow 1$ ) in the electronic ground state, requiring a dynamic dipole moment (associated with a change in the dipole moment during the vibrational motion) [28]. In contrast, Raman spectroscopy is based on photon scattering by molecules and has its origin in the electronic polarization caused by monochromatic visible radiation [28, 29]. Therefore, a vibrational mode is Raman active if the polarizability is modulated during the vibration [28, 29]. Strict selection rules exist for both spectroscopies, sometimes leading to complementary detection [29]. For example, the vibration of the homopolar diatomic molecule H<sub>2</sub> is not IR active (due to the absence of a fluctuating dipole associated with the symmetric stretching), but strongly Raman active. However, once the molecule interacts with the MOF, it undergoes a perturbation that slightly polarizes the originally symmetric molecule and makes it weakly IR active. This perturbation is usually accompanied by a red-shift of the H–H stretching modes, located at 4161.1 and 4155 cm<sup>-1</sup> for para and ortho H<sub>2</sub>, respectively [30]. For the linear molecule CO<sub>2</sub>, the symmetric stretch mode ( $\nu_1$ ) is Raman active but not IR active, whereas the antisymmetric modes ( $\nu_2$  and  $\nu_3$ ) are IR active [29].

Based on these principles, IR and Raman spectroscopy can be very useful tools to characterize the nature of

host/guest interactions [31–34] in MOFs. Particularly valuable information can be gained by identifying perturbations of the IR active modes. For example, the first spectroscopic evidence for the formation of an electron-donor–acceptor (EDA) complex between CO<sub>2</sub> and functional groups of MOFs was observed in a MOF of type MIL-53 and reported in later studies of the adsorption of CO<sub>2</sub> in amino-based MOFs [32, 33]. The adsorption of CO<sub>2</sub> molecules in MIL-53 leads to a modest red-shift from  $-10$  to  $-15$  cm<sup>-1</sup> of the stretching mode  $\nu_3$  and to a splitting of the bending mode  $\nu_2$  due to the removal of degeneracy of the in-plane and out-of-plane bends [32]. A similar splitting of  $\nu_2$  modes is common in many electron-donor–acceptor complexes of CO<sub>2</sub> with organic solvents or polymers possessing electron-donating functional groups—e.g., carbonyl groups—due to the interaction of the carbon atom of CO<sub>2</sub> as the electron acceptor [35, 36]. Moreover, significant perturbations of both  $\nu(\text{OH})$  and  $\sigma(\text{OH})$  bands of hydroxyl groups ( $\nu(\text{OH}) = 19$  cm<sup>-1</sup> and  $\sigma(\text{OH}) = 30$  cm<sup>-1</sup>) suggest that oxygen atoms of the framework hydroxyl group act as the electron donor [32].

As evident from these examples (and many others), it is clear that IR and Raman spectroscopy, by themselves and even without the aid of theoretical calculations, can often provide insight into the interactions between guest molecules and the MOF. However, as we will see in the next section, in other cases the ‘blind’ application of these spectroscopic techniques can lead to a significant misinterpretation of the experimental data obtained. This can happen when IR and Raman spectroscopy are used as *indirect* probes—i.e. deducing other physical properties of the system from a simple red- or blue-shift in the spectrum. In such cases, theory and computer simulations are essential to derive a complete understanding, as they provide *direct* access to many properties of the system, and often provide interpretations that are unexpected from simple correlations in the experimental data.

## 2.2. Difficulty of IR and Raman spectroscopy to describe small molecule adsorption in MOFs

Despite the high sensitivity of spectroscopy to molecular interactions with the MOF, attention must be paid when interpreting the data to extract information about the interaction from vibrational frequency shifts, intensities and line widths [37, 38]. For example, it is commonly accepted that the magnitude of the IR shift of small adsorbed molecules in MOFs is directly related to their adsorption energy, and thus the IR shift can be used indirectly to estimate the relative adsorption energies. However, in our recent IR spectroscopy study of molecular hydrogen in a number of different MOF compounds [37], we find that there is no clear correlation between H<sub>2</sub> adsorption energies (determined by isotherm measurements) and the magnitude of the H<sub>2</sub> stretch shift. In fact, metal-formate M<sub>3</sub>(HCOO)<sub>6</sub> (M = Co, Ni and Mn) compounds with the highest adsorption energy have the lowest hydrogen IR shift. In this case, we find that the IR shift is dominated by the environment (organic ligand, metal center and structure) [37], rather than by the adsorption energy to the metal.

Similarly, integrated areas for the specific IR bands were long considered to be directly correlated with the amount (loading) of adsorbed molecules, assuming that the dipole moment of the adsorbed species is not affected by loading or site geometry [39–41]. Based on this assumption, variable temperature IR was used to measure the absorbance of IR bands (including that of H<sub>2</sub> molecules) and estimate the adsorption energy [39, 41]. However, our theoretical and experimental findings for H<sub>2</sub> molecules in MOF74 with unsaturated metal centers indicate that large variations in the induced dipole moment take place as a function of loading, due to the interaction among adsorbed molecules [38]. In the case of Mg-MOF74, the effective charge of H<sub>2</sub> at the metal sites weakens (from 0.021 *e* to 0.015 *e* as the loading increases from 1 to 12 H<sub>2</sub>/primitive cell) as the neighboring sites are occupied. Thus, the IR intensity is reduced by 50%, since it is proportional to the square of the effective charge or the dynamic dipole moment [38]. These findings suggest that the integrated areas of IR bands do not always correlate with the amount of H<sub>2</sub> adsorbed, and possible variations in dynamic dipole moments have to be taken into account.

In summary, IR and Raman spectroscopy can be very helpful tools when studying small molecule adsorption in MOFs. However, extreme caution is necessary when utilizing those methods to make assumptions about adsorption energies or loadings, as illustrated in the examples given above. Under these circumstances, theoretical input using first-principles calculations—specifically capable of dealing with van der Waals interactions—is critical to interpret experimental observations correctly.

## 2.3. Experimentation

Zecchina and coworkers first used transmission IR spectroscopy to study the fundamental aspects of the interaction between H<sub>2</sub> and MOFs, mainly in the low-temperature (<300 K) and low-pressure regime. By means of the variable temperature infrared (VTIR) spectroscopy method, the adsorption enthalpy was derived by measuring the intensity of absorption bands as a function of temperature [40, 42]. However, caution must be used when using the VTIR method since the dipole moment might change as a function of loading, as pointed out above. More recent work [24, 37, 38, 43] has investigated a series of small molecules (H<sub>2</sub>, CO<sub>2</sub>, CH<sub>4</sub>, SO<sub>2</sub>, H<sub>2</sub>O, etc) using *in situ* IR absorption spectroscopy to quantify the effect of their interaction with different types of MOFs in a wide range of pressures (from 50 mTorr to 55 bar) and temperatures (10–423 K). In order to perform the IR measurements at and above room temperature, a portion (~10 mg) of MOF was lightly pressed onto a KBr support and mounted into a high-temperature, high-pressure cell (Specac product number P/N 5850c) and further heated in vacuum for activation. During the annealing, the removal of solvent molecules was monitored by *in situ* IR spectroscopy. Then, the activated sample was cooled to specific temperatures in order to perform the measurements at specific pressure gas exposures. Measurements were

performed in transmission using a liquid-N<sub>2</sub> cooled InSb/MCT detector. Similar measurements were also performed in a Janis PTSHI series cold refrigerator (CCR) system for low-temperature studies (<298 K). In addition to transmission IR, diffuse reflectance infrared Fourier transform spectroscopy (DRIFTS) was employed to investigate the dynamics of H<sub>2</sub> molecules adsorbed within the MOF74 compounds [33, 34]. Furthermore, DRIFTS has also been used to study the interactions between CO<sub>2</sub> and functional groups on the organic ligands of some MOFs under the controlled *in situ* cell environment [44–46].

Most recently, *in situ* Raman spectroscopy was also used to study the structural response mechanism of flexible metal organic frameworks Zn<sub>2</sub>(bpdC)<sub>2</sub>bpee [bpdC = 4,40-biphenyl dicarboxylate and bpee = 1,2-bis(4-pyridyl)ethylene] upon CO<sub>2</sub>, N<sub>2</sub> and hydrocarbon molecules adsorption [47, 48]. In this case, Raman spectroscopy is more suitable because the phonon modes of the MOFs do not overwhelm the spectra as they do in the case of IR spectra, which include a large number of combination and overtone bands. By integrating a Linkam FTIR600 cooling/heating stage, the activated sample was measured under a controlled temperature and gas environment. The changes on specific bonds in the MOF structure, monitored by Raman spectroscopy, were correlated to the MOF structural changes and the guest–host interactions.

### 3. Computer simulations as a tool to interpret complex spectroscopic experiments

#### 3.1. *Ab initio* modeling of materials

While very successful classical modeling techniques exist, such as force field simulations, which are suitable for studying very large systems, they are not capable of describing the electronic structure of materials and the intricate role it plays in many processes. In the case of MOF materials, we are most interested in electronic-structure changes during the adsorption and desorption of small molecules in their cavities, as well as a number of catalytic processes. As such, unless the cost is prohibitive, *ab initio* modeling techniques are the methods of choice. For an overview of widely used materials-modeling techniques, ranging from classical approaches to high-level quantum-chemistry methods, see [49].

Modeling MOF materials with *ab initio* methods presents a particular challenge. The adsorption/desorption of small molecules in MOFs is often governed by physisorption, i.e. weak van der Waals forces, which are difficult to capture correctly with *ab initio* methods. Correlated high-level quantum-chemistry approaches, such as Møller–Plesset perturbation theory and coupled-cluster methods [50], can describe van der Waals interactions, but their computational cost limits them to small systems (~100 and ~30 atoms, respectively [51]) and their application to large periodic systems, such as the MOFs of interest here, is unpractical [52–57].

Density functional theory (DFT) [58], on the other hand, has a much more favorable computational cost and can be used for systems with up to 1000 atoms—in

linear-scaling DFT even up to 1000 000 atoms [51]. It is also easily implemented with periodic plane-wave basis sets, such that treating periodic systems becomes trivial. Unfortunately, with standard exchange–correlation functionals, DFT cannot reliably describe van der Waals interactions [59–62], a phenomenon where charge fluctuations in one part of the system correlate with fluctuations in another, resulting in an attractive force that is a *truly nonlocal correlation effect* [63]. It follows that standard local and semi-local functionals, such as LDA and GGA, cannot reliably account for these nonlocal effects and yield qualitatively erroneous predictions [64–67]. While very promising extensions exist [64], most notably DFT-D [68, 69], DFT-SAPT [70–72] and C<sub>6</sub>-based methods [73, 74], they are semi-empirical, perturbative and not seamlessly self-consistent density functionals.

#### 3.2. *vdW-DF: a good compromise between cost and accuracy*

We have overcome this problem and include van der Waals forces self-consistently in DFT [26] in the form of a van der Waals density functional (vdW-DF). Its accuracy is comparable to high-level quantum-chemistry approaches [75–77]. vdW-DF goes beyond standard DFT to include a *truly nonlocal correlation*  $E_c^{nl}$  in the exchange–correlation energy  $E_{xc}$ ,

$$E_{xc}[n] = E_x^{\text{revPBE}}[n] + E_c^{\text{LDA}}[n] + E_c^{nl}[n], \quad (1)$$

$$E_c^{nl}[n] = \frac{1}{2} \int d^3r d^3r' n(\vec{r})\phi(\vec{r}, \vec{r}')n(\vec{r}'), \quad (2)$$

where  $n$  is the electron density and revPBE [78] and LDA [79] are standard functionals.  $E_c^{nl}$  is determined by the kernel  $\phi$ , which is a complicated function of the densities and their gradients at  $\vec{r}$  and  $\vec{r}'$ , first developed by Langreth *et al* [25]. With the corresponding exchange–correlation potential  $v_c^{nl}(\vec{r}) = \delta E_c^{nl}[n]/\delta n(\vec{r})$  [26], the method becomes self-consistent and permits the calculation of atomic forces—essential for structural optimization and molecular-dynamics simulations. Like high-level quantum-chemical methods, vdW-DF precludes bias through a full, self-consistent solution of the coupled Schrödinger equations for all valence electrons. Calculations automatically include direct and induced electrostatic effects, charge transfer effects and effects due to the non-nuclear centrality of the dispersion interaction as well as its deviations from the inverse sixth power at smaller than asymptotic separations.

vdW-DF can be implemented in standard plane-wave electronic-structure codes exploiting an efficient Fast Fourier transform algorithm [80]. This algorithm scales like standard DFT, and for large systems compute times are negligibly longer than for GGA calculations. We routinely use our own implementation to study hydrogen-storage materials with 300–400 atoms per unit cell [81, 82]. In particular, we have successfully used vdW-DF to study a variety of phenomena in MOF materials, achieving remarkable agreement with experiment [24, 43, 48, 83–90].

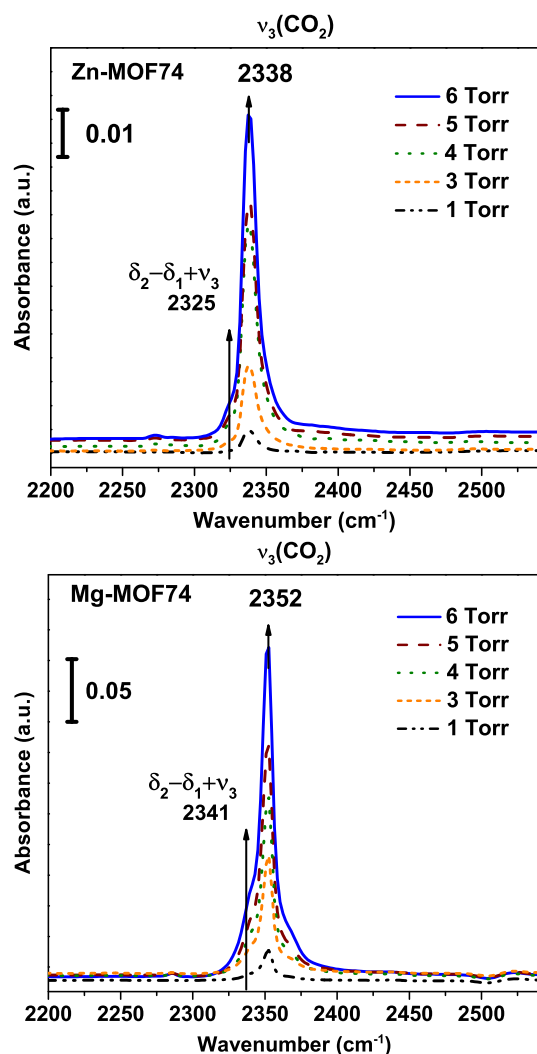


**Figure 1.** IR absorption spectra of CO<sub>2</sub> adsorbed into Zn-MOF74 (top) and into Mg-MOF74 (bottom) at changing CO<sub>2</sub> pressure (1–6 Torr). (Reprinted with permission from [83]. © 2012 American Physical Society.)

### 3.3. Comparison between vdW-DF simulations and experiment

In MOF adsorption studies, there are ample opportunities for theory and experiment to interact. It is almost straightforward to compare vdW-DF optimized structures with diffraction experiments [91–93]. Of more interest is the comparison of calculated adsorption energies with measured heats of adsorption [94–98]. As pointed out above, IR spectroscopy can be a very powerful method to study the loading of MOFs, but caution is necessary. From the theoretical side, while the full calculation of IR spectra is possible [99], it is much easier and typically sufficient to calculate the IR peak positions—this has been done in a number of studies and shows very good agreement with experiment [83, 85, 97]. Comparison with IR experiments has also been made for vdW-DF calculations of small molecule diffusion [86]. vdW-DF calculations for an exhaustive list of elastic and transport properties of MOFs are also compared with experiment [92, 100, 101].

**Table 1.** Vibrational frequencies (cm<sup>-1</sup>) of CO<sub>2</sub> physisorbed in MOF74. Data taken from [83].

	System	Bending mode (ν <sub>2</sub> )	Asym. stretch mode (ν <sub>3</sub> )
Exp.	Free CO <sub>2</sub>	667	2349
	Mg-MOF74	658	2352
	Zn-MOF74	658	2338
Calc.	Free CO <sub>2</sub>	646.6	2288.5
	Mg-MOF74	636.6	2288.0
	Zn-MOF74	637.6	2280.4

## 4. Examples of successful combined experimental/theoretical studies

### 4.1. Studying adsorption mechanisms of small molecules in MOFs

It has been shown that MOFs with unsaturated metal centers, such as MOF74 and HKUST-1, exhibit a fast and specific CO<sub>2</sub> absorption, which is a desirable property for capturing applications [47, 102–104]. Therefore, understanding their absorption mechanisms is critical for the rational design of improved MOFs. In this subsection we discuss and analyze CO<sub>2</sub> absorption in MOF74. We will show that the vdW-DF approach is critical in order to understand and correctly explain the corresponding experimental results. As an example, we review CO<sub>2</sub> absorption in Zn-MOF74 and Mg-MOF74 and show how the frequency of the asymmetric and stretching modes are modified upon adsorption [83].

The experimental IR absorption spectra results in figure 1 show that the unperturbed asymmetric stretch mode of CO<sub>2</sub> (2349 cm<sup>-1</sup>) undergoes shifts of -11 cm<sup>-1</sup> and +3 cm<sup>-1</sup> upon adsorption on Zn-MOF74 and Mg-MOF74, respectively. But, what causes this shift? To answer this question, *ab initio* calculations were performed utilizing vdW-DF, finding three factors contributing to this shift, i.e. (i) the change in the CO<sub>2</sub> molecule length, (ii) the asymmetric distortion of the CO<sub>2</sub> molecule, and (iii) the direct influence of the metal center.

In table 1, we compare the IR spectroscopy data with results from frozen-phonon vdW-DF calculations, where the CO<sub>2</sub> molecule was adsorbed at the metal site of MOF74. In particular, the frozen-phonon calculations for the bending mode of CO<sub>2</sub> give a change in frequency of approximately -9 cm<sup>-1</sup> during adsorption on either metal, in excellent agreement with the experimental results. Furthermore, the calculations show that the asymmetric stretch mode of the CO<sub>2</sub> molecule exhibits red-shifts of -0.5 cm<sup>-1</sup> and -8.1 cm<sup>-1</sup> when adsorbed on Mg-MOF74 and Zn-MOF74, respectively, in reasonable agreement with the changes of +3 cm<sup>-1</sup> and -11 cm<sup>-1</sup> measured in experiments.

According to vdW-DF calculations [83], the CO<sub>2</sub> molecule binds more strongly to Mg-MOF74 than to Zn-MOF74, in agreement with experimental findings. Furthermore, the distance between the metal center and the CO<sub>2</sub> molecule is smaller in Mg-MOF74 than in Zn-MOF74. Also, the CO<sub>2</sub> molecule experiences a larger distortion upon adsorption in Mg-MOF74, see table 1 in [83]. Therefore, it is

surprising that the frequency shift of the asymmetric stretching mode (see  $\nu_3$  in table 1) for CO<sub>2</sub> in Mg-MOF74 is smaller compared with that in Zn-MOF74, and a deeper investigation of what causes this peculiar result is warranted. As mentioned above, this result can be explained with the help of theory.

We will start with the change in the molecule length: in order to analyze this effect, phonon calculations of the free CO<sub>2</sub> molecule were performed, where its length was set to the value when adsorbed in the MOF, keeping the carbon atom centered. Using this approach, frequency shifts of  $-1.6\text{ cm}^{-1}$  and  $-3.7\text{ cm}^{-1}$  were obtained for the cases of Mg- and Zn-MOF74, respectively. It is interesting to see that in the case of Mg-MOF74, the molecule experiences a marginal elongation of  $0.0003\text{ \AA}$ , while in the case of Zn-MOF74 an elongation of  $0.0009\text{ \AA}$  takes place. That is, the molecule that experiences the larger elongation exhibits the larger red-shift, as suggested by common sense.

The effect corresponding to the molecule's asymmetric distortion was studied by placing the CO<sub>2</sub> molecule exactly at the same geometry as when adsorbed in the MOF, but removing the surrounding MOF. By doing this, the only contributions to the change in frequency come from the elongation of the CO<sub>2</sub> molecule and the asymmetric distortion of the carbon atom. The former has been reported in the paragraph above, so that the latter can easily be calculated. In this way, we find the shifts corresponding to the induced asymmetry of the CO<sub>2</sub> molecule to be  $1.1\text{ cm}^{-1}$  and  $0.7\text{ cm}^{-1}$  for Mg-MOF74 and Zn-MOF74, respectively.

Finally, the effect of the metal center was studied by placing the free, undistorted CO<sub>2</sub> molecule at the metal adsorption site with the same position and angle of the adsorbed system. By doing this, the change in frequency has its highest contribution coming from the oxygen-metal interaction. Using this configuration, the results show a frequency shift of the asymmetric stretching mode of the CO<sub>2</sub> molecule of  $-5\text{ cm}^{-1}$  for the Zn-MOF74 system. On the other hand, for Mg-MOF74 the frequency shift has a negligible value of  $-0.6\text{ cm}^{-1}$ . This is a striking result, since Mg and Zn have very similar valence structure with 3s and 4s electrons as the outermost valence states. This result shows that the fully occupied semi-core 3d electrons in Zn have an important effect on the interaction with the adsorbed CO<sub>2</sub> molecules. Similar results are found in Co- and Ni-MOF74 structures. To shed more light on this situation, a charge-density analysis was performed, finding a depletion of electrons around the Zn atom upon adsorption of the CO<sub>2</sub> molecule, while this depletion was not present for Mg-MOF74. Thus, the depletion of charge is an effect of the Zn d orbitals, which, in turn, also influences the charge distribution in the adsorbed CO<sub>2</sub> molecule. Via this mechanism, the Zn d orbitals indirectly affect the IR frequency shift of the adsorbed CO<sub>2</sub> molecule—explaining the differences between Mg-MOF74 and Zn-MOF74.

In summary, this van der Waals study of small molecule adsorption on MOFs is driven by experimental IR data. But, it is clear that the reasons for the observed IR frequency shifts are not necessarily intuitive and can only be explained with the help of detailed first-principles simulations.

#### 4.2. Studying the chemical stability of MOFs under humid conditions

The stability of MOFs under humid conditions [105–110] is of great importance for the implementation of these systems in various applications and devices. For example, the MOF5 structure is very sensitive to water and its hydrogen uptake properties become compromised when it is exposed to humidity in ambient air. So, how can we design new MOFs that keep their desired properties while being water resistant? In the case of MOF5, Yeng *et al* [105] reported the synthesis of methyl- and 2,5-dimethyl-modified versions. By introducing methyl into the linkers, the structure becomes less reactive to water and retains the same hydrogen uptake properties of MOF5 up to four days after being exposed to ambient air. While this is a specific case, resting on the specific interaction of water and H<sub>2</sub> with the methyl-modified linkers, it can easily be generalized and it is again the interaction of small molecules—in this case water—with the MOF that is the focus of much ongoing research.

In this subsection, we review efforts to understand the MOF–water interaction, using as an example the prototypical metal organic framework M(bdc)(ted)<sub>0.5</sub> (M = Cu, Zn, Ni, Co; bdc = 1,4-benzenedicarboxylate; ted = triethylenediamine). This MOF has shown promising properties towards the adsorption of gases, such as H<sub>2</sub>, CO<sub>2</sub>, and CH<sub>4</sub> [111–113]. M(bdc)(ted)<sub>0.5</sub> exhibits thermal stability up to 282 °C, is highly porous, the H<sub>2</sub> adsorption is exceptionally high, and it can also adsorb a large amount of hydrocarbons. This system was first synthesized and reported by Dybtsev *et al* in [113] and we will review here its water stability, as originally studied in [43]. A characteristic building block of this particular MOF is the incorporated ‘paddle-wheel’ building-block ted (triethylenediamine), which acts as a linker. In the presence of water, this paddle-wheel structure can be extracted from the framework and replaced by water molecules, forming M-MOF2 (we will refer to it as MOF2), as can be seen in figure 2. Obviously, with its normal linker missing, the M(bdc)(ted)<sub>0.5</sub> structure loses stability and, in most cases, undergoes a non-reversible phase transition.

Figure 3 shows the powder x-ray diffraction (XRD) pattern of four hydrated M(bdc)(ted)<sub>0.5</sub> systems (M = Cu, Zn, Co and Ni) after exposure to 9.5 Torr of D<sub>2</sub>O vapor and the corresponding activated (pristine) M(bdc)(ted)<sub>0.5</sub> samples. Concerning the Cu(bdc)(ted)<sub>0.5</sub> system, the XRD pattern confirms that the system is stable after exposure to D<sub>2</sub>O gas up to a pressure of 6 Torr, see figure S10 in the supporting information of [43]. However, the top left panel of figure 3 shows that all the x-ray peaks are shifted to higher angles, except for the [001] peak, indicating that the Cu(bdc)(ted)<sub>0.5</sub> system is partially hydrolyzed by the D<sub>2</sub>O molecules. Even though the structure is only partially hydrolyzed, the original Cu(bdc)(ted)<sub>0.5</sub> structure cannot be recovered after evacuation of water at a temperature of 150 °C. In contrast, the left bottom panel of figure 3 clearly indicates that the Zn(bdc)(ted)<sub>0.5</sub> system transforms into MOF2 after hydration. This transformation starts with the detachment of the ted group and the subsequent bonding of the D<sub>2</sub>O molecules to the Zn<sup>2+</sup> apical sites of the paddle-wheel building units

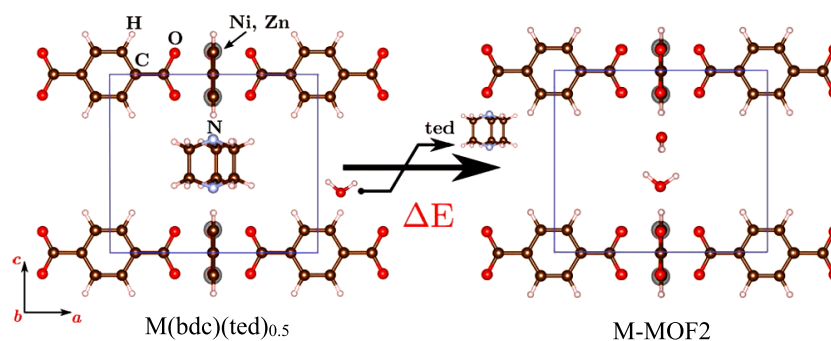


**Figure 2.** Scheme adopted for water insertion in  $M(\text{bdc})(\text{ted})_{0.5}$  ( $M = \text{Zn}, \text{Ni}$ ), where the ted group has been substituted by two water molecules. (Reprinted with permission from [43]. © 2012 American Chemical Society.)

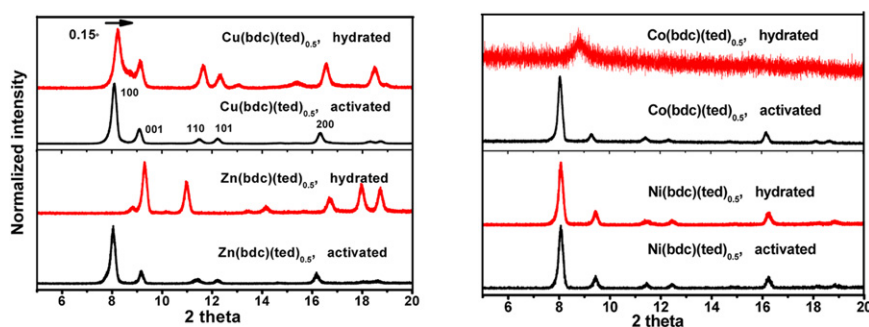


**Figure 3.** Powder x-ray patterns of activated (pristine) and hydrated  $M(\text{bdc})(\text{ted})_{0.5}$  ( $M = \text{Cu}, \text{Zn}, \text{Co}$  and  $\text{Ni}$ ) after exposure to 9.5 Torr of  $\text{D}_2\text{O}$  vapor. (Reprinted with permission from [43]. © 2012 American Chemical Society.)

through their oxygen atoms. Concerning the  $\text{Ni}(\text{bdc})(\text{ted})_{0.5}$  and  $\text{Co}(\text{bdc})(\text{ted})_{0.5}$  systems under humid conditions, the right bottom and right upper panels of figure 3 indicate that the  $\text{Ni}(\text{bdc})(\text{ted})_{0.5}$  maintains its structure after been exposed to 9.5 Torr of  $\text{D}_2\text{O}$  vapor, while the  $\text{Co}(\text{bdc})(\text{ted})_{0.5}$  is completely destroyed after exposure. Furthermore, the  $\text{Co}(\text{bdc})(\text{ted})_{0.5}$  structure cannot be recovered after annealing in vacuum up to  $150^\circ\text{C}$ , see figure S13 in the supplemental material of [43].

In order to explain the previous experimental results and give a clear explanation of how water interacts with the  $M(\text{bdc})(\text{ted})_{0.5}$ , we review computational results obtained in [43] concerning the  $\text{Ni}(\text{bdc})(\text{ted})_{0.5}$  and  $\text{Zn}(\text{bdc})(\text{ted})_{0.5}$  systems. The energy  $\Delta E$  needed to extract the paddle wheel and replace it with water molecules was calculated using the vdW-DF formalism as

$$\Delta E_{M(\text{bdc})(\text{ted})_{0.5}} = E[M(\text{bdc})(\text{ted})_{0.5}] + E[n \text{H}_2\text{O}] - E[\text{MOF2} + n \text{H}_2\text{O}] - 1/2 E[(\text{ted})], \quad (3)$$

where  $n$  is the number of water molecules in the MOF,  $E[M(\text{bdc})(\text{ted})_{0.5}]$  is the energy of the MOF with no water molecules in it (as seen in the left panel of figure 2),  $E[n \text{H}_2\text{O}]$  is the energy of  $n$  water molecules,  $E[\text{MOF2} + n \text{H}_2\text{O}]$  is the energy of the  $M(\text{bdc})(\text{ted})_{0.5}$  where the ‘exciting’ ted has been replaced with  $n$  water molecules (right panel of figure 2) and  $E[(\text{ted})]$  is the energy of the ted. Table 2 shows the energies required to substitute the ted in the Zn and  $\text{Ni}(\text{bdc})(\text{ted})_{0.5}$  structures by 2, 4, 6, 8 and 10 water molecules. Note that negative  $\Delta E$  values indicate that the

**Table 2.** Computed  $\Delta E_{M(\text{bdc})(\text{ted})_{0.5}}$  and  $\Delta E_{M-\text{MOF2}}$  ( $\text{kJ mol}^{-1} \text{cell}^{-1}$ ) as a function of the number of water molecules per cell. Note that the basic MOF2 structure already contains two water molecules. Data taken from [43].

$\text{H}_2\text{O}/\text{cell}$	$\Delta E_{M(\text{bdc})(\text{ted})_{0.5}}$			$\Delta E_{M-\text{MOF2}}$		
	Zn	Ni	$\Delta$	Zn	Ni	$\Delta$
2	43.1	85.5	42.4	—	—	—
4	-5.3	4.2	9.5	-53.6	-77.1	-23.5
6	-21.4	-17.1	4.3	-53.7	-68.4	-14.7
8	-31.3	-24.0	7.3	-56.1	-52.4	3.7
10	-35.0	-45.2	-10.2	-54.5	-55.3	-0.8

replacement is energetically favorable. The table shows that  $\text{Ni}(\text{bdc})(\text{ted})_{0.5}$  is more resistant to water than  $\text{Zn}(\text{bdc})(\text{ted})_{0.5}$ , as found in the spectra in figure 3, and the hydration of the latter is a spontaneous process. This is due to the strong H bonds between the water molecules, which stabilizes the coordination of the Zn metal centers. On the other hand, in the case of  $\text{Ni}(\text{bdc})(\text{ted})_{0.5}$ ,  $\Delta E_{M(\text{bdc})(\text{ted})_{0.5}}$  becomes negative only when the number of water molecules is six or greater.

Alternatively, one can calculate the energy  $\Delta E_{M-\text{MOF2}}$  required for hydration of the MOF2 structure with  $n$  water molecules, using:

$$\Delta E_{M-\text{MOF2}} = E[\text{MOF2}] + E[n \text{H}_2\text{O}] - E[\text{MOF2} + n \text{H}_2\text{O}]. \quad (4)$$

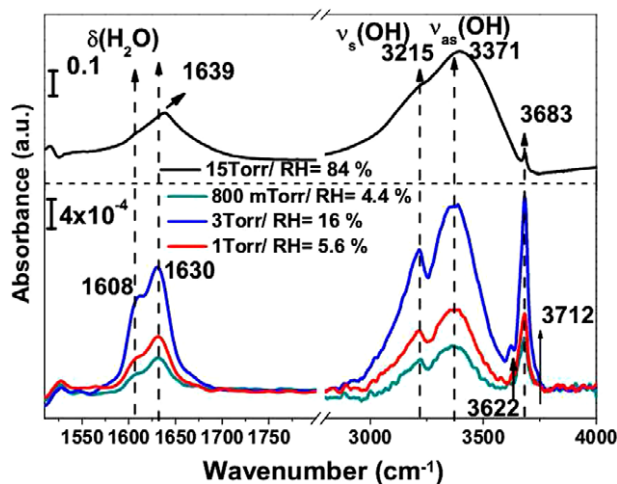


**Figure 4.** IR absorption spectra of water exposure in FMOF1 as a function of pressure. Absorption spectra are referenced to dehydrated FMOF1 in vacuum. The top panel shows exposure at 15 Torr, while the bottom part shows exposure at lower pressures (800 mTorr–3 Torr). (Reprinted with permission from [24]. © 2013 American Chemical Society.)

Here,  $E[\text{MOF2}]$  is the energy of the  $\text{M}(\text{bdc})(\text{ted})_{0.5}$ , where the ted has been replaced by two molecules of water; the other terms in the equation have been previously defined, see equation (3). The right hand side of table 2 shows that for MOF2 the hydration of the Zn and Ni systems is a spontaneous process with an energy gain of approximately  $-55 \text{ kJ mol}^{-1} \text{ cell}^{-1}$  for higher loadings. This trend is almost independent of the metal.

In conclusion, the computational results explain the experimental findings in [43], indicating that the structural stability of the system depends on the amount of water present in the MOF. At lower loadings the system is stable, while at higher loadings the interaction of water with the paddle wheel leads to the irreversible decomposition of the structure.

#### 4.3. Studying the formation of water clusters in fluorinated MOFs

The large internal surface area of MOFs makes them ideal for catalysis and fuel-cell applications, which have attracted a surge of interest [10–12, 16, 114, 115]. While some progress has been made—for example, Hurd *et al* [116] show intriguing results for  $\beta$ -PCMOF2 (proton conducting metal organic framework 2), capable of proton transport under anhydrous conditions at  $150^\circ\text{C}$ —in general, the low hydrothermal and chemical stability of MOFs prevents their implementation in catalytic and fuel-cell systems. In the recent past, thus, concerted efforts have focused on increasing the hydrothermal and chemical stability of MOFs [109, 117, 118].

A promising approach to increase the chemical and hydrothermal stability is fluorinated MOFs (FMOFs), where the H atoms have been replaced by F atoms [119–121]. Yang *et al* report interesting results for FMOF1, showing that the hydrogen-desorption isotherm does not follow the path of the adsorption isotherm [119], in fact, it shows an abrupt drop in the adsorption density at 14 bar. The authors highlight the fact

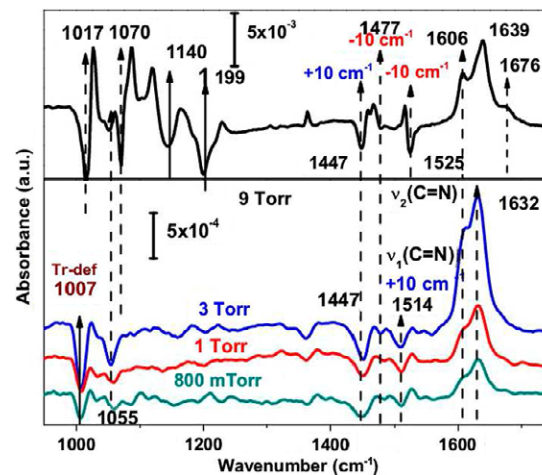


**Figure 5.** IR absorption spectra of  $\text{H}_2\text{O}$  adsorbed in FMOF1 showing the bending modes of adsorbed water as a function of pressure. Top part shows the IR absorption spectrum at 9 Torr. (Reprinted with permission from [24]. © 2013 American Chemical Society.)

that this behavior would allow FMOF1 to adsorb  $\text{H}_2$  at high pressures and store it at low pressures.

In general, the walls of FMOF systems are hydrophobic, leading to an interesting side effect: the weak interaction of water molecules with the FMOF enhances the creation of water clusters inside its pores. In this subsection, we review the formation and behavior of water clusters inside FMOF1, as reported in [24]. As in previous sections, an understanding of the weak molecular interactions inside this system was gained by a combination of vdW-DF calculations and IR absorption spectra of water-exposed FMOF1 as a function of pressure. Note that the interaction between water molecules has a significant van der Waals component, which is well captured with vdW-DF [122], while the electrostatic interaction is suppressed by the wall hydrophobicity of FMOF1.

Experimental isotherm measurements of FMOF1 show that the adsorption of water is negligible compared to the water adsorption in other systems [121]. Furthermore, at low water pressures (800 mTorr–3 Torr), the IR adsorption measurements of  $\text{H}_2\text{O}$  adsorbed on FMOF1 show two peaks corresponding to red- ( $-13 \text{ cm}^{-1}$ ) and blue-shifts ( $+9 \text{ cm}^{-1}$ ) of the unperturbed scissor vibration mode ( $1621 \text{ cm}^{-1}$ ) of the water molecule, as can be seen in figure 4. On the other hand, as the pressure is increased to 9 Torr, new peaks associated with scissor vibration modes appear at  $1639$  and  $1676 \text{ cm}^{-1}$ , as can be seen in the top panel of figure 5.

In order to elucidate the appearance and nature of these peaks, vdW-DF vibration calculations were performed for various water clusters, i.e. the water dimer, trimer, tetramer, pentamer and ice; the results are shown in figure 6. Figure 6(a) shows the calculated modes convolved with Gaussian functions of  $20 \text{ cm}^{-1}$  bandwidth, while panel (b) shows single-frequency values represented by peaks of  $1 \text{ cm}^{-1}$  width. As expected, from the figure it can be seen that the bigger the water cluster, the greater the number of scissor modes. It is also important to note that for pressures under 3 Torr, the scissor vibrational modes in figure 4 span from

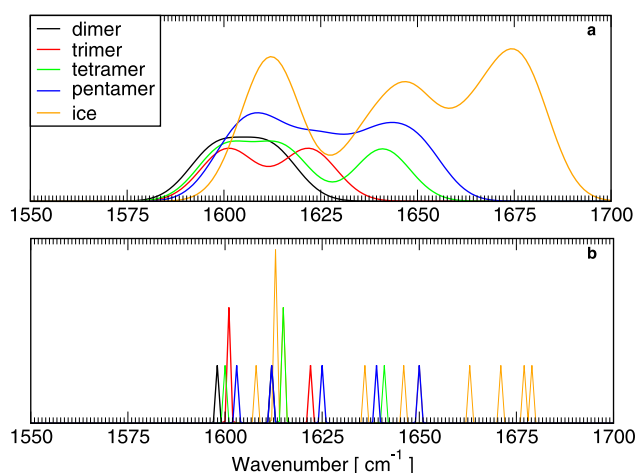


**Figure 6.** (a) Gaussian convolution (with bandwidth of  $20\text{ cm}^{-1}$ ) of bending mode frequencies for various cluster sizes. (b) Single-frequency values represented by peaks of  $1\text{ cm}^{-1}$  width, as reported by previous vdW-DF calculations on gas-phase water clusters [122]. (Reprinted with permission from [24]. © 2013 American Chemical Society.)

$1600$  to  $1650\text{ cm}^{-1}$ . This matches the theoretical frequency windows of both the tetramer and pentamer, as seen in the top panel of figure 6. It follows that the water clusters formed inside FMOF1 under low pressures ( $<3$  Torr) are comprised of no more than five water molecules. This conclusion is also supported by the water adsorption energies on the FMOF1, see table 2 in [24]. Note that, in principle, up to 61 water molecules can be accommodated inside the pores of FMOF1. On the other hand, the experimentally observed peak located at  $1676\text{ cm}^{-1}$  in figure 5 can be associated with hydrogen-bonded water molecules or water clusters larger than five water molecules—see the orange line in the top panel of figure 6. It is important to note that this peak is only visible at high pressures.

In summary, while the IR spectroscopy data of water-exposed FMOF1 showed the appearance of new peaks, it was only with the help of vdW-DF calculations that a clear assignment to particular water clusters could be made. Note that this finding is likely to have a tremendous impact on atmospheric sciences, which seek to study the existence and properties of such clusters. In the normal atmosphere, water cluster concentration decays exponentially with the aggregate size, making clusters larger than the trimer often difficult to observe. FMOF1 solves this problem and provides a simple environment to create and confine even larger clusters.

#### 4.4. Studying small molecule diffusion in MOFs

MOFs have attracted a lot of attention due their promising properties concerning the storage of hydrogen and capture of  $\text{CO}_2$  [9], among others. However, for the effectiveness of all such applications, it is necessary to get guest molecules deep into the bulk of the MOF, or vice versa, have them diffuse out. As such, the diffusivity of the guest molecule through the porous material plays a major role in these processes and is critical for the understanding and rational design of new

MOFs. The topic of small molecule diffusion in MOFs has thus been the target of many theoretical studies [123–129]. For example, in [128], Haldoupis *et al* identified key elements in the MOF's pore structure and via molecular dynamic simulations they were able to predict the Henry constant and the activation energy for several guest molecules. In particular, the authors were able to identify several materials with promising properties towards the separation of gases, such as  $\text{H}_2$ ,  $\text{CO}_2$ , and  $\text{CH}_4$ . However, in their study, the authors assume that the MOFs are rigid structures, which can be a serious limitation, as we know that some MOFs experience a significant change in their structure upon adsorption of the guest molecules or other external stimuli due to their high flexibility.

In this subsection we review a combined *in situ* IR/vdW-DF study of small molecule diffusion in Mg-MOF74, as described in [87]. MOF74 was chosen for this study due to its unsaturated metal centers, which makes it highly reactive towards the adsorption of small molecules. Furthermore, Mg-MOF74 has shown promising properties towards the adsorption of  $\text{CO}_2$  compared to other MOFs.

We start by showing results concerning the adsorption energies of  $\text{H}_2$ ,  $\text{CO}_2$ , and  $\text{H}_2\text{O}$  in the Mg-MOF74 structure, see table 3. This table shows that for low to moderate loadings the interaction between adsorbate molecules is negligible, except for  $\text{H}_2\text{O}$  adsorption, where the repulsion between the H atoms of the water molecules slightly debilitates the  $\text{H}_2\text{O}$  binding to the MOF. The adsorption energies for the adsorption of  $\text{H}_2$  and  $\text{CO}_2$ , obtained using the vdW-DF approach, are in excellent agreement with the experimental values of  $-0.11 \pm 0.003\text{ eV}$  [98] and  $-0.49 \pm 0.010\text{ eV}$  [104], respectively. Although not the focus of that particular study, table 3 also reveals a common problem of many MOFs: the adsorption energy of water (due to its large dipole moment) is typically significantly higher compared to, for example,  $\text{H}_2$  and  $\text{CO}_2$ . Thus, the presence of even small traces of water is a serious impediment to possible applications and devices, as anticipated in the previous section. Details about this problem are discussed in [90]. In addition to adsorption energies, calculations of the vibrational spectra show a frequency change after adsorption of  $\Delta\nu_{\text{H}_2} = -30\text{ cm}^{-1}$ ,  $\Delta\nu_{\text{CO}_2} = -13\text{ cm}^{-1}$  and  $\Delta\nu_{\text{H}_2\text{O}} = -103\text{ cm}^{-1}$ , in remarkable agreement with the IR spectroscopy measurements of  $\Delta\nu_{\text{H}_2} = -36\text{ cm}^{-1}$ ,  $\Delta\nu_{\text{CO}_2} = -8\text{ cm}^{-1}$  and  $\Delta\nu_{\text{H}_2\text{O}} = -99\text{ cm}^{-1}$ . Experimentally, there is also a small difference in the frequency change between low and high loading, resulting in red-shifts of  $-3$  and  $-15\text{ cm}^{-1}$  for the asymmetric stretch modes of  $\text{CO}_2$  and  $\text{H}_2\text{O}$  respectively (see supplemental material of [87]). Computationally, we find  $\Delta\nu_{\text{CO}_2} = -1\text{ cm}^{-1}$  and  $\Delta\nu_{\text{H}_2\text{O}} = -18\text{ cm}^{-1}$ , again in excellent agreement with experiment.

The diffusion of small molecules ( $\text{H}_2$ ,  $\text{CO}_2$  and  $\text{H}_2\text{O}$ ) through the MOF is a complex process. An appropriate description of such processes typically requires computationally expensive first-principles molecular dynamic simulations. However, here we were able to avoid the use of molecular dynamics by finding four different diffusion paths that capture the important molecular transport mechanisms responsible for the macroscopic diffusion of  $\text{H}_2$ ,  $\text{CO}_2$  and

**Table 3.** Adsorption energies  $\Delta E$  of molecules in Mg-MOF74 in eV. Two different loadings are considered, i.e. one molecule per unit cell (low loading) and six molecules per unit cell (high loading). In addition, adsorption energies corrected for the zero-point energy ( $\Delta E_{ZPE}$ ) and thermal contribution ( $\Delta H_{298}$  at 298 K) are given in eV. Data taken from [87].

Molecule	Loading	$\Delta E$	$\Delta E_{ZPE}$	$H_{298}$
H <sub>2</sub>	1	-0.15	-0.15	-0.15
	6	-0.16	-0.16	-0.16
CO <sub>2</sub>	1	-0.50	-0.49	-0.50
	6	-0.50	-0.49	-0.50
H <sub>2</sub> O	1	-0.79	-0.76	-0.76
	6	-0.76	-0.73	-0.73

H<sub>2</sub>O in the MOF structure. These four paths are: (a) the guest molecule, adsorbed on one metal center, travels circularly from one metal center to the next. Note that this mechanism is not responsible for molecular transport into the MOF, but nevertheless is an important process for redistributing the molecular load. (b) The guest molecule, adsorbed on the metal center, diffuses along the *c*-axis to the next metal center. (c) The guest molecule travels through the center of the MOF's channel, where all the metal centers are occupied by the same type of guest molecules. (d) The guest molecule, adsorbed on one of the metal centers, travels along the *c*-axis through a barrier made by adsorbed molecules and is adsorbed at the equivalent metal center two unit cells further down. See figure 7 for a graphical representation of these four diffusion paths. For these paths, diffusion barriers were then calculated utilizing vdW-DF combined with the climbing-image nudged elastic band (NEB) approach.

The energy barriers of the four diffusion paths are plotted in figure 8. Note that diffusion barriers corrected for the zero-point energy were also calculated, but are not reproduced here. From the figure it can be seen that water has the highest energy barrier for diffusion. Again, the presence of water inside the MOF is a serious issue, as the barrier for it to diffuse out is rather large. As expected, the energy barriers are comparable to the adsorption energies. In panel (a), it can be seen that a local minimum is located at 58% of the path for CO<sub>2</sub> diffusion. This local minimum has its origins in the presence of a secondary adsorption site in the MOF. Due to its low depth (5 meV), the secondary adsorption site is occupied only at high loadings. This secondary adsorption site for the CO<sub>2</sub> molecule was first reported by Queen *et al* in [130], where the authors conducted neutron powder diffraction experiments on the Mg-MOF74 as a function of the CO<sub>2</sub> loading. Paths (b)–(d) aim to simulate the diffusion of the guest molecule into the MOF. Note that the diffusion barriers in path (c) are ten times lower than the ones obtained in paths (a)–(d). This indicates that the interaction between the guest molecules in the middle of the channel and the ones adsorbed at the metals sites is small. Furthermore, it is important to highlight that the diffusion energy barrier of CO<sub>2</sub> in figure 8(c), i.e. 0.04 eV, becomes 0.03 eV when corrected for the zero-point energy. This value is in excellent agreement with the 0.03 eV energy barrier measured experimentally by Bao *et al* in [131].

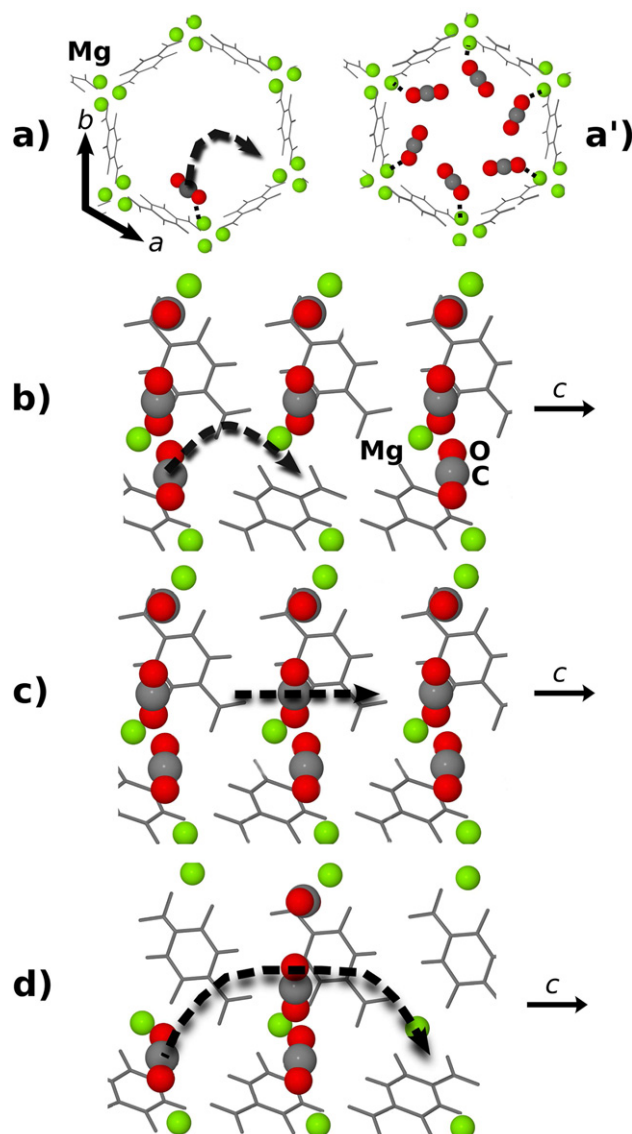


**Figure 7.** Graphical representation of the diffusion mechanisms considered in this study, shown for the case of CO<sub>2</sub>. (a) and (a') are views directly along the *c*-axis of the hexagonal Mg-MOF74 cell, where one (low loading) and six CO<sub>2</sub> (high loading) are adsorbed. (b)–(d) are views perpendicular to the *c*-axis. In panel (b) the guest molecule, adsorbed on a metal center, diffuses along the *c*-axis to the next metal center. In panel (c) the guest molecule travels along the center of the MOF channel, while all the metal centers are occupied by the same type of guest molecule. In panel (d) the guest molecule, adsorbed on one of the metal centers, travels along the *c*-axis through a barrier made of other adsorbed molecules and is adsorbed again at the equivalent metal center two unit cells further down. Dashed lines indicate the diffusion paths. (Reprinted with permission from [87]. © 2012 American Physical Society.)

In addition to vdW-DF calculations, *in situ* IR time-resolved spectroscopy measurements of the diffusion of CO<sub>2</sub> and H<sub>2</sub>O in Mg-MOF74 were performed. When the experiments were first performed, the results were difficult to understand. In the case of CO<sub>2</sub>, at first we observed a red-shift in the vibration frequency (asymmetric mode) of the guest molecules. As time passes, the IR spectrum measurements show a second shift (blue-shift) in the vibration frequencies

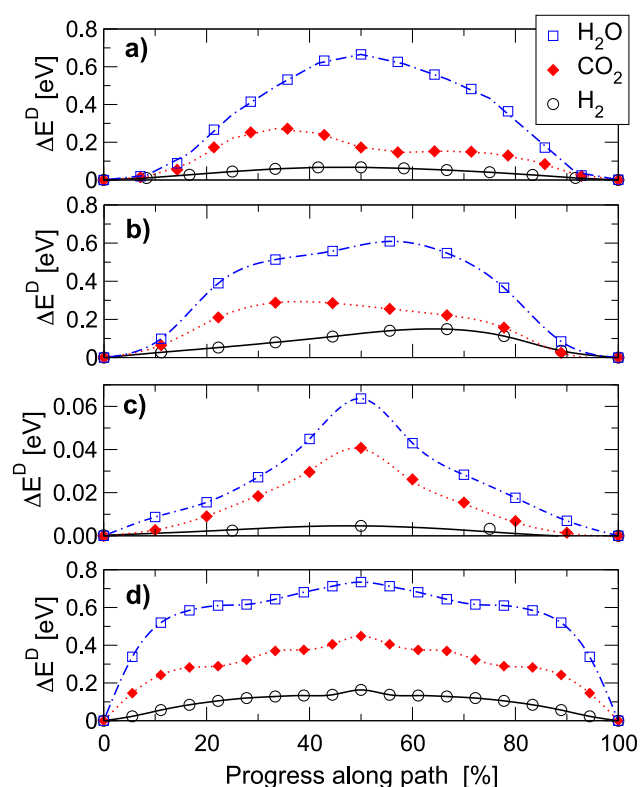


**Figure 8.** Diffusion profiles (in eV) for the diffusion processes of H<sub>2</sub>, CO<sub>2</sub>, and H<sub>2</sub>O in Mg-MOF74 according to the mechanisms in figure 7. (Reprinted with permission from [87]. © 2012 American Physical Society.)

of the guest molecules, leading to the original IR spectrum. The analogous behavior is observed for the corresponding experiment with H<sub>2</sub>O. With the help of theory, we were able to construct a model that explains these effects. At first, molecules entering the MOF mostly adsorb in the pores close to the surface and ‘clog’ those. This causes the first experimentally observed red-shift. Those pores become highly loaded, which we were able to deduce from the calculated difference in frequency shift from the low- and high-loading situations. Then, after some time, molecules start to diffuse deeper into the MOF using mechanism (c), diffusing from pores with a high concentration of guest molecules to pores with lower concentration. This results in the second shift observed, i.e. blue-shifting back to the original spectrum.

To test our model, we compare the experimental timescale for the CO<sub>2</sub> and H<sub>2</sub>O cases. The experiments show that it takes approximately two hours for the H<sub>2</sub>O molecules and 22 min for the CO<sub>2</sub> molecules to go from the high-loading regime to the low-loading regime. The ratio between these two times is 5.45. On the other hand, having calculated the corresponding diffusion barriers (and calculating the pre-exponential factor in the Arrhenius equation with the help of transition-state theory), we can compute the same ratio and find based purely on our *ab initio* calculations a value of 5.43, validating our theoretical accuracy and transport model.

In summary, as in the previous subsections, only the combination of experiment and theory was able to present a complete picture of small molecule diffusion in

MOF74. The theoretical atomistic model for the molecular transport explains experimental IR macroscopic evidence. The simulations also clarify the two-state mechanism, observed experimentally, which controls the macroscopic diffusion of these molecules in MOF74.

## 5. Summary and outlook

In this work, we have shown several examples of how the synergy of IR and Raman spectroscopy techniques, together with *ab initio* calculations at the DFT level utilizing vdW-DF, allow us to give a complete description of the van der Waals binding and interaction between guest molecules and the MOF. While originally many studies of MOFs focused on the adsorption of H<sub>2</sub> and CO<sub>2</sub>, at the moment we see a vast expansion of this field, including many other molecules of interest, such as SO<sub>2</sub> and NO<sub>2</sub> [89, 132–135]. Interesting effects are also being studied, such as a pressure-dependent gate opening of MOFs [48, 136–138] and the response of MOFs to a variety of external stimuli. Due to the versatile building-block nature of MOFs, an almost innumerable number of MOFs might exist. However, more fundamental research is necessary to understand their properties and tailor them according to our needs. Nonetheless, at this point we have probably only seen a glimpse of their applicability for future applications and devices.

## Acknowledgment

This work was entirely supported by Department of Energy Grant No. DE-FG02-08ER46491.

## References

- [1] Zhao D, Yuan D and Zhou H-C 2008 The current status of hydrogen storage in metal–organic frameworks *Energy Environ. Sci.* **1** 222–35
- [2] Sun D, Ma S, Ke Y, Collins D J and Zhou H-C 2006 An interweaving MOF with high hydrogen uptake *J. Am. Chem. Soc.* **128** 3896–7
- [3] Rosi N L, Eckert J, Eddaoudi M, Vodak D T, Kim J, O’Keeffe M and Yaghi O M 2003 Hydrogen storage in microporous metal–organic frameworks *Science* **300** 1127–11279
- [4] Furukawa H, Miller M A and Yaghi O M 2007 Independent verification of the saturation hydrogen uptake in MOF-177 and establishment of a benchmark for hydrogen adsorption in metal–organic frameworks *J. Mater. Chem.* **17** 3197–204
- [5] An J and Rosi N L 2010 Tuning MOF CO<sub>2</sub> adsorption properties via cation exchange *J. Am. Chem. Soc.* **132** 5578–9
- [6] Liu J, Thallapally P K, Peter McGrail B, Brown D R and Liu J 2012 Progress in adsorption-based CO<sub>2</sub> capture by metal–organic frameworks *Chem. Soc. Rev.* **41** 2308–22
- [7] Mallick A, Saha S, Pachfule P, Roy S and Banerjee R 2010 Selective CO<sub>2</sub> and H<sub>2</sub> adsorption in a chiral magnesium-based metal organic framework (Mg-MOF) with open metal sites *J. Mater. Chem.* **20** 9073–80
- [8] Grajciar L, Wiersum A D, Llewellyn P L, Chang J-S and Nachtigall P 2011 Understanding CO<sub>2</sub> adsorption in

- CuBTC MOF: comparing combined DFT-*ab initio* calculations with microcalorimetry experiments *J. Phys. Chem. C* **115** 17925–33
- [9] Pera-Titus M 2014 Porous inorganic membranes for CO<sub>2</sub> capture: present and prospects *Chem. Rev.* **114** 1413–92
- [10] Farha O K, Shultz A M, Sarjeant A A, Nguyen S T and Hupp J T 2011 Active-site-accessible, porphyrinic metal–organic framework materials *J. Am. Chem. Soc.* **133** 5652–5
- [11] Lee J Y, Farha O K, Roberts J, Scheidt K A, Nguyen S T and Hupp J T 2009 Metal–organic framework materials as catalysts *Chem. Soc. Rev.* **38** 1450–9
- [12] Shultz A M, Farha O K, Hupp J T and Nguyen S T 2009 A catalytically active, permanently microporous MOF with metalloporphyrin struts *J. Am. Chem. Soc.* **131** 4204–5
- [13] Kreno L E, Leong K, Farha O K, Allendorf M, Van Duyne R P and Hupp J T 2012 Metal–organic framework materials as chemical sensors *Chem. Rev.* **112** 1105–25
- [14] Stroppa A, Barone P, Jain P, Perez-Mato J M and Picozzi S 2013 Hybrid improper ferroelectricity in a multiferroic and magnetoelectric metal organic framework *Adv. Mater.* **25** 2284–90
- [15] Stroppa A, Jain P, Barone P, Marsman M, Perez-Mato J M, Cheetham A K, Kroto H W and Picozzi S 2011 Electric control of magnetization and interplay between orbital ordering and ferroelectricity in a multiferroic metal organic framework *Angew. Chem. Int. Edn* **50** 5847–50
- [16] Kuppler R J, Timmons D J, Fang Q-R, Li J-R, Makal T A, Young M D, Yuan D, Zhao D, Zhuang W and Zhou H-C 2009 Potential applications of metal–organic frameworks *Coord. Chem. Rev.* **253** 3042–66
- [17] Stock N and Biswas S 2012 Synthesis of metal–organic frameworks (MOFs): routes to various MOF topologies, morphologies, and composites *Chem. Rev.* **112** 933–69
- [18] Rowsell J L C, Millward A R, Park K S and Yaghi O M 2004 Hydrogen sorption in functionalized metal–organic frameworks *J. Am. Chem. Soc.* **126** 5666–7
- [19] Yang Q *et al* 2013 A water stable metal–organic framework with optimal features for CO<sub>2</sub> capture *Angew. Chem. Int. Edn* **52** 10316–20
- [20] Taylor J M, Dawson K W and Shimizu G K H 2013 A water-stable metal–organic framework with highly acidic pores for proton-conducting applications *J. Am. Chem. Soc.* **135** 1193–6
- [21] Li Y, Ju Z, Wu B and Yuan D 2013 A water and thermally stable metal–organic framework featuring selective CO<sub>2</sub> adsorption *Cryst. Growth Des.* **13** 4125–30
- [22] Han S S, Choi S-H and van Duin A C T 2010 Molecular dynamics simulations of stability of metal–organic frameworks against H<sub>2</sub>O using the ReaxFF reactive force field *Chem. Commun.* **46** 5713–5
- [23] Demessence A, D’Alessandro D M, Foo M L and Long J R 2009 Strong CO<sub>2</sub> binding in a water-stable, triazolate-bridged metal–organic framework functionalized with ethylenediamine *J. Am. Chem. Soc.* **131** 8784–6
- [24] Nijem N *et al* 2013 Water cluster confinement and methane adsorption in the hydrophobic cavities of a fluorinated metal–organic framework *J. Am. Chem. Soc.* **135** 12615–26
- [25] Dion M, Rydberg H, Schröder E, Langreth D C and Lundqvist B I 2004 Van der Waals density functional for general geometries *Phys. Rev. Lett.* **92** 246401
- [26] Thonhauser T, Cooper V R, Li S, Puzder A, Hyldgaard P and Langreth D C 2007 Van der Waals density functional: self-consistent potential and the nature of the van der Waals bond *Phys. Rev. B* **76** 125112
- [27] Lee K, Murray É D, Kong L, Lundqvist B I and Langreth D C 2010 Higher-accuracy van der Waals density functional *Phys. Rev. B* **82** 081101
- [28] Nakamoto K 2009 *Infrared and Raman Spectra of Inorganic and Coordination Compounds* 6th edn (Hoboken, NJ: Wiley)
- [29] Ferraro J R, Nakamoto K and Brown C W 2003 *Introductory Raman Spectroscopy* 2nd edn (San Diego, CA: Academic)
- [30] Welsh H L 1969 The pressure-induced infrared spectrum of hydrogen and its application to the study of planetary atmospheres *J. Atmos. Sci.* **26** 835–40
- [31] Lamberti C, Zecchina A, Groppo E and Bordiga S 2010 Probing the surfaces of heterogeneous catalysts by *in situ* IR spectroscopy *Chem. Soc. Rev.* **39** 4951–5001
- [32] Vimont A, Travert A, Bazin P, Lavalley J-C, Daturi M, Serre C, Ferey G, Bourrelly S and Llewellyn P L 2007 Evidence of CO<sub>2</sub> molecule acting as an electron acceptor on a nanoporous metal–organic-framework MIL-53 or Cr<sup>3+</sup>(OH)(O<sub>2</sub>C–C<sub>6</sub>H<sub>4</sub>–CO<sub>2</sub>) *Chem. Commun.* 3291–3
- [33] Gascon J, Aktay U, Hernandez-Alonso M D, van Klink G P M and Kapteijn F 2009 Amino-based metal–organic frameworks as stable, highly active basic catalysts *J. Catal.* **261** 75–87
- [34] Stavitski E, Pidko E A, Couck S, Remy T, Hensen E J M, Weckhuysen B M, Denayer J, Gascon J and Kapteijn F 2011 Complexity behind CO<sub>2</sub> capture on NH<sub>2</sub>-MIL-53(Al) *Langmuir* **27** 3970–6
- [35] Dobrowolski J Cz and Jamroz M H 1992 Infrared evidence for CO<sub>2</sub> electron donor–acceptor complexes *J. Mol. Struct.* **275** 211–9
- [36] Kazarian S G, Vincent M F, Bright F V, Liotta C L and Eckert C A 1996 Specific intermolecular interaction of carbon dioxide with polymers *J. Am. Chem. Soc.* **118** 1729–36
- [37] Nijem N, Veyan J-F, Kong L, Li K, Pramanik S, Zhao Y, Li J, Langreth D and Chabal Y J 2010 Interaction of molecular hydrogen with microporous metal organic framework materials at room temperature *J. Am. Chem. Soc.* **132** 1654–64
- [38] Nijem N, Veyan J-F, Kong L, Wu H, Zhao Y, Li J, Langreth D C and Chabal Y J 2010 Molecular hydrogen ‘pairing’ interaction in a metal organic framework system with unsaturated metal centers (MOF-74) *J. Am. Chem. Soc.* **132** 14834–48
- [39] Bordiga S, Regli L, Bonino F, Groppo E, Lamberti C, Xiao B, Wheatley P S, Morris R E and Zecchina A 2007 Adsorption properties of HKUST-1 toward hydrogen and other small molecules monitored by IR *Phys. Chem. Chem. Phys.* **9** 2676–85
- [40] Vitillo J G, Regli L, Chavan S, Ricchiardi G, Spoto G, Dietzel P D C, Bordiga S and Zecchina A 2008 Role of exposed metal sites in hydrogen storage in MOFs *J. Am. Chem. Soc.* **130** 8386–96
- [41] Garrone E and Otero Arean C 2005 Variable temperature infrared spectroscopy: a convenient tool for studying the thermodynamics of weak solid–gas interactions *Chem. Soc. Rev.* **34** 846–57
- [42] Bordiga S, Vitillo J G, Ricchiardi G, Regli L, Cocina D, Zecchina A, Arstad B, Bjørgen M, Hafizovic J and

- Lillerud K P 2005 Interaction of hydrogen with MOF-5 *J. Phys. Chem. B* **109** 18237–42
- [43] Tan K, Nijem N, Canepa P, Gong Q, Li J, Thonhauser T and Chabal Y J 2012 Stability and hydrolyzation of metal organic frameworks with paddle-wheel SBUs upon hydration *Chem. Mater.* **24** 3153–67
- [44] FitzGerald S A, Burkholder B, Friedman M, Hopkins J B, Pierce C J, Schloss J M, Thompson B and Rowsell J L C 2011 Metal-specific interactions of H<sub>2</sub> adsorbed within isostructural metal–organic frameworks *J. Am. Chem. Soc.* **133** 20310–8
- [45] FitzGerald S A, Hopkins J, Burkholder B, Friedman M and Rowsell J L C 2010 Quantum dynamics of adsorbed normal- and para-H<sub>2</sub>, HD, and D<sub>2</sub> in the microporous framework MOF-74 analyzed using infrared spectroscopy *Phys. Rev. B* **81** 104305
- [46] Windisch Jr C F, Thallapally P K and Peter McGrail B 2009 Adsorption of CO<sub>2</sub> on CO<sub>3</sub>[CO<sup>III</sup>(CN)<sub>6</sub>]<sub>2</sub> using DRIFTS *Spectrochim. Acta A* **74** 629–34
- [47] Nijem N *et al* 2011 Understanding the preferential adsorption of CO<sub>2</sub> over N<sub>2</sub> in a flexible metal–organic framework *J. Am. Chem. Soc.* **133** 12849–57
- [48] Nijem N, Wu H, Canepa P, Marti A, Balkus K J, Thonhauser T, Li J and Chabal Y J 2012 Tuning the gate opening pressure of metal–organic frameworks (MOFs) for the selective separation of hydrocarbons *J. Am. Chem. Soc.* **134** 15201–4
- [49] Kolb B and Thonhauser T 2012 Molecular biology at the quantum level: can modern density functional theory forge the path? *Nano LIFE* **02** 1230006
- [50] Szabo A and Ostlund N S 1996 *Modern Quantum Chemistry: Introduction to Advanced Electronic Structure Theory* (Mineola, NY: Dover)
- [51] Head-Gordon M and Artacho E 2008 Chemistry on the computer *Phys. Today* **61** 58–63
- [52] Marsman M, Grüneis A, Paier J and Kresse G 2009 Second-order Møller–Plesset perturbation theory applied to extended systems. I. Within the projector-augmented-wave formalism using a plane wave basis set *J. Chem. Phys.* **130** 184103
- [53] Booth G H, Grüneis A, Kresse G and Alavi A 2012 Towards an exact description of electronic wavefunctions in real solids *Nature* **493** 365–70
- [54] Grüneis A, Marsman M and Kresse G 2010 Second-order Møller–Plesset perturbation theory applied to extended systems. II. Structural and energetic properties *J. Chem. Phys.* **133** 074107
- [55] Usvyat D, Civalieri B, Maschio L, Dovesi R, Pisani C and Schütz M 2011 Approaching the theoretical limit in periodic local MP2 calculations with atomic-orbital basis sets: the case of LiH *J. Chem. Phys.* **134** 2141050
- [56] Ayala P Y, Kudin K N and Scuseria G E 2001 Atomic orbital Laplace-transformed second-order Møller–Plesset theory for periodic systems *J. Chem. Phys.* **115** 9698–707
- [57] Maschio L, Usvyat D, Manby F R, Casassa S, Pisani C and Schütz M 2007 Fast local-MP2 method with density-fitting for crystals. I. Theory and algorithms *Phys. Rev. B* **76** 075101
- [58] Hohenberg P and Kohn W 1964 Inhomogeneous electron gas *Phys. Rev.* **136** B864–87
- [59] Shevlin S A and Guo Z X 2009 Density functional theory simulations of complex hydride and carbon-based storage materials *Chem. Soc. Rev.* **38** 211–25
- [60] Hobza P 2008 Stacking interaction *Phys. Chem. Chem. Phys.* **10** 2581–3
- [61] Šponer J, Riley K E and Hobza P 2008 Nature and magnitude of aromatic stacking of nucleic acid bases *Phys. Chem. Chem. Phys.* **10** 2595–610
- [62] Černý J and Hobza P 2007 Non-covalent interactions in biomacromolecules *Phys. Chem. Chem. Phys.* **9** 5291–303
- [63] Langreth D C *et al* 2009 A density functional for sparse matter *J. Phys.: Condens. Matter* **21** 084203
- [64] French R H *et al* 2010 Long range interactions in nanoscale science *Rev. Mod. Phys.* **82** 1887–944
- [65] Kristyán S and Pulay P 1994 Can (semi)local density functional theory account for the London dispersion forces? *Chem. Phys. Lett.* **229** 175–80
- [66] Pérez-Jordá J M, Becke A D and San-Fabián E 1994 Automatic numerical integration techniques for polyatomic molecules *J. Chem. Phys.* **100** 6520–34
- [67] Meijer E J and Sprik M 1996 A density-functional study of the intermolecular interactions of benzene *J. Chem. Phys.* **105** 8684–9
- [68] Grimme S 2004 Accurate description of van der Waals complexes by density functional theory including empirical corrections *J. Comput. Chem.* **25** 1463–73
- [69] Grimme S 2006 Semiempirical GGA-type density functional constructed with a long-range dispersion correction *J. Comput. Chem.* **27** 1787–99
- [70] Heßelmann A and Jansen G 2003 The helium dimer potential from a combined density functional theory and symmetry-adapted perturbation theory approach using an exact exchange–correlation potential *Phys. Chem. Chem. Phys.* **5** 5010–4
- [71] Misquitta A J and Szalewicz K 2002 Intermolecular forces from asymptotically corrected density functional description of monomers *Chem. Phys. Lett.* **357** 301–6
- [72] Williams H L and Chabalowski C F 2001 Using Kohn–Sham orbitals in symmetry-adapted perturbation theory to investigate intermolecular interactions *J. Phys. Chem. A* **105** 646–59
- [73] Tkatchenko A and Scheffler M 2009 Accurate molecular van der Waals interactions from ground-state electron density and free-atom reference data *Phys. Rev. Lett.* **102** 073005
- [74] Tkatchenko A, DiStasio Jr R A, Head-Gordon M and Scheffler M 2009 Dispersion-corrected Møller–Plesset second-order perturbation theory *J. Chem. Phys.* **131** 094106
- [75] Cooper V R, Thonhauser T, Puzder A, Schröder E, Lundqvist B I and Langreth D C 2008 Stacking interactions and the twist of DNA *J. Am. Chem. Soc.* **130** 1304–8
- [76] Cooper V R, Thonhauser T and Langreth D C 2008 An application of the van der Waals density functional: hydrogen bonding and stacking interactions between nucleobases *J. Chem. Phys.* **128** 204102
- [77] Li H W, Kikuchi K, Nakamori Y, Ohba N, Miwa K, Towata S and Orimo S 2008 Dehydrogenating and rehydrogenating processes of well-crystallized Mg(BH<sub>4</sub>)<sub>2</sub> accompanying with formation of intermediate compounds *Acta Mater.* **56** 1342–7
- [78] Zhang Y and Yang W 1998 Comment on ‘generalized gradient approximation made simple’ *Phys. Rev. Lett.* **80** 890

- [79] Perdew J P and Wang Y 1992 Accurate and simple analytical representation of the electron-gas correlation-energy *Phys. Rev. B* **45** 13244–9
- [80] Román-Pérez G and Soler J M 2009 Efficient implementation of a van der Waals density functional: application to double-wall carbon nanotubes *Phys. Rev. Lett.* **103** 096102
- [81] Bil A, Kolb B, Atkinson R, Pettifor D G, Thonhauser T and Kolmogorov A N 2011 van der Waals interactions in the ground state of  $\text{Mg}(\text{BH}_4)_2$  from density functional theory *Phys. Rev. B* **83** 224103
- [82] Li Qi, Kolb B, Román-Pérez G, Soler J M, Yndurain F, Kong L, Langreth D C and Thonhauser T 2011 *Ab initio* energetics and kinetics study of  $\text{H}_2$  and  $\text{CH}_4$  in the SI clathrate hydrate *Phys. Rev. B* **84** 153103
- [83] Yao Y, Nijem N, Li J, Chabal Y J, Langreth D C and Thonhauser T 2012 Analyzing the frequency shift of physisorbed  $\text{CO}_2$  in metal organic framework materials *Phys. Rev. B* **85** 064302
- [84] Li Q and Thonhauser T 2012 A theoretical study of the hydrogen-storage potential of  $(\text{H}_2)_4\text{CH}_4$  in metal organic framework materials and carbon nanotubes *J. Phys.: Condens. Matter* **24** 424204
- [85] Nijem N, Canepa P, Kong L, Wu H, Li J, Thonhauser T and Chabal Y J 2012 Spectroscopic characterization of van der Waals interactions in a metal organic framework with unsaturated metal centers: MOF-74-Mg *J. Phys.: Condens. Matter* **24** 424203
- [86] Canepa P, Chabal Y J and Thonhauser T 2013 When metal organic frameworks turn into linear magnets *Phys. Rev. B* **87** 094407
- [87] Canepa P, Nijem N, Chabal Y J and Thonhauser T 2013 Diffusion of small molecules in metal organic framework materials *Phys. Rev. Lett.* **110** 026102
- [88] Lopez M G, Canepa P and Thonhauser T 2013 NMR study of small molecule adsorption in MOF-74-Mg *J. Chem. Phys.* **138** 154704
- [89] Tan K, Canepa P, Gong Q, Liu J, Johnson D H, Dyevoich A, Thallapally P K, Thonhauser T, Li J and Chabal Y J 2013 Mechanism of preferential adsorption of  $\text{SO}_2$  into two microporous paddle wheel frameworks  $\text{M}(\text{bdc})(\text{ted})_{0.5}$  *Chem. Mater.* **25** 4653–62
- [90] Canepa P, Arter C A, Conwill E M, Johnson D H, Shoemaker B A, Soliman K Z and Thonhauser T 2013 High-throughput screening of small-molecule adsorption in MOF *J. Mater. Chem. A* **1** 13597–604
- [91] Walker A M, Civalieri B, Slater B, Mellot-Draznieks C, Corá F, Zicovich-Wilson C M, Román-Pérez G, Soler J M and Gale J D 2010 Flexibility in a metal–organic framework material controlled by weak dispersion forces: the bistability of MIL-53(AI) *Angew. Chem. Int. Edn* **49** 7501–3
- [92] Kleis J, Lundqvist B I, Langreth D C and Schröder E 2007 Towards a working density-functional theory for polymers: first-principles determination of the polyethylene crystal structure *Phys. Rev. B* **76** 100201
- [93] Ziambaras E, Kleis J, Schröder E and Hyldgaard P 2007 Potassium intercalation in graphite: a van der Waals density-functional study *Phys. Rev. B* **76** 155425
- [94] Lee K, Berland K, Yoon M, Andersson S, Schröder E, Hyldgaard P and Lundqvist B I 2012 Benchmarking van der Waals density functionals with experimental data: potential-energy curves for  $\text{H}_2$  molecules on  $\text{Cu}(111)$ , (100) and (110) surfaces *J. Phys.: Condens. Matter* **24** 424213
- [95] Poloni R, Smit B and Neaton J B 2012  $\text{CO}_2$  capture by metal–organic frameworks with van der Waals density functionals *J. Phys. Chem. A* **116** 4957–64
- [96] Chakarova-Käck S D, Schröder E, Lundqvist B I and Langreth D C 2006 Application of van der Waals density functional to an extended system: adsorption of benzene and naphthalene on graphite *Phys. Rev. Lett.* **96** 146107
- [97] Kong L, Cooper V R, Nijem N, Li K, Li J, Chabal Y J and Langreth D C 2009 Theoretical and experimental analysis of  $\text{H}_2$  binding in a prototypical metal–organic framework material *Phys. Rev. B* **79** 081407
- [98] Zhou W, Wu H and Yildirim T 2008 Enhanced  $\text{H}_2$  adsorption in isostructural metal–organic frameworks with open metal sites: strong dependence of the binding strength on metal ions *J. Am. Chem. Soc.* **130** 15268–9
- [99] Kong L, Chabal Y J and Langreth D C 2011 First-principles approach to rotational-vibrational frequencies and infrared intensity for  $\text{H}_2$  adsorbed in nanoporous materials *Phys. Rev. B* **83** 121402
- [100] Langreth D C, Dion M, Rydberg H, Schröder E, Hyldgaard P and Lundqvist B I 2005 Van der Waals density functional theory with applications *Int. J. Quantum Chem.* **101** 599–610
- [101] Londero E and Schröder E 2010 Role of van der Waals bonding in the layered oxide  $\text{V}_2\text{O}_5$ : first-principles density-functional calculations *Phys. Rev. B* **82** 054116
- [102] Dietzel P D C, Johnsen R E, Fjellvag H, Bordiga S, Groppo E, Chavan S and Blom R 2008 Adsorption properties and structure of  $\text{CO}_2$  adsorbed on open coordination sites of metal–organic framework  $\text{Ni}_2(\text{dhtp})$  from gas adsorption, IR spectroscopy and x-ray diffraction *Chem. Commun.* 5125–7
- [103] Wu H, Simmons J M, Srinivas G, Zhou W and Yildirim T 2010 Adsorption sites and binding nature of  $\text{CO}_2$  in prototypical metal–organic frameworks: a combined neutron diffraction and first-principles study *J. Phys. Chem. Lett.* **1** 1946–51
- [104] Valenzano L, Civalieri B, Chavan S, Palomino G T, Areán C O and Bordiga S 2010 Computational and experimental studies on the adsorption of  $\text{CO}$ ,  $\text{N}_2$ , and  $\text{CO}_2$  on Mg-MOF-74 *J. Phys. Chem. C* **114** 11185–91
- [105] Yang J, Grzech A, Mulder F M and Dingemans T J 2011 Methyl modified MOF-5: a water stable hydrogen storage material *Chem. Commun.* **47** 5244–6
- [106] Wu T, Shen L, Luebbbers M, Hu C, Chen Q, Ni Z and Masel R I 2010 Enhancing the stability of metal–organic frameworks in humid air by incorporating water repellent functional groups *Chem. Commun.* **46** 6120–2
- [107] Greathouse J A and Allendorf M D 2006 The interaction of water with MOF-5 simulated by molecular dynamics *J. Am. Chem. Soc.* **128** 10678–9
- [108] Ma D, Li Y and Li Z 2011 Tuning the moisture stability of metal–organic frameworks by incorporating hydrophobic functional groups at different positions of ligands *Chem. Commun.* **47** 7377–9
- [109] Low J J, Benin A I, Jakubczak P, Abrahamian J F, Faheem S A and Willis R R 2009 Virtual high throughput screening confirmed experimentally: porous coordination polymer hydration *J. Am. Chem. Soc.* **131** 15834–42

- [110] Saha D and Deng S 2010 Structural stability of metal organic framework MOF-177 *J. Phys. Chem. Lett.* **1** 73–8
- [111] Chen Y F, Lee J Y, Babarao R, Li J and Jiang J W 2010 A highly hydrophobic metal–organic framework Zn(BDC)(TED)<sub>0.5</sub> for adsorption and separation of CH<sub>3</sub>OH/H<sub>2</sub>O and CO<sub>2</sub>/CH<sub>4</sub>: an integrated experimental and simulation study *J. Phys. Chem. C* **114** 6602–9
- [112] Lee J Y, Olson D H, Pan L, Emge T J and Li J 2007 Microporous metal–organic frameworks with high gas sorption and separation capacity *Adv. Funct. Mater.* **17** 1255–62
- [113] Dybtsev D N, Chun H and Kim K 2004 Rigid and flexible: a highly porous metal–organic framework with unusual guest-dependent dynamic behavior *Angew. Chem. Int. Edn* **43** 5033–6
- [114] Kitagawa H 2009 Metal–organic frameworks: transported into fuel cell *Nature Chem.* **1** 689–90
- [115] Llabrés i Xamena F X, Corma A and Garcia H 2007 Applications for metal–organic frameworks (MOFs) as quantum dot semiconductors *J. Phys. Chem. C* **111** 80–5
- [116] Hurd J A, Vaidhyanathan R, Thangadurai V, Ratcliffe C I, Moudrakovski I L and Shimizu G K H 2009 Anhydrous proton conduction at 150 °C in a crystalline metal–organic framework *Nature Chem.* **1** 705–10
- [117] Ma S, Wang X-S, Yuan D and Zhou H-C 2008 A coordinatively linked Yb metal–organic framework demonstrates high thermal stability and uncommon gas-adsorption selectivity *Angew. Chem. Int. Edn* **47** 4130–3
- [118] Sun D, Ma S, Ke Y, Petersen T M and Zhou H-C 2005 Synthesis, characterization, and photoluminescence of isostructural Mn, Co, and Zn MOFs having a diamondoid structure with large tetrahedral cages and high thermal stability *Chem. Commun.* 2663–5
- [119] Yang C, Wang X and Omary M A 2007 Fluorous metal–organic frameworks for high-density gas adsorption *J. Am. Chem. Soc.* **129** 15454–5
- [120] Yang C, Wang X and Omary M A 2009 Crystallographic observation of dynamic gas adsorption sites and thermal expansion in a breathable fluorous metal–organic framework *Angew. Chem. Int. Edn* **48** 2500–5
- [121] Yang C, Kaipa U, Mather Q Z, Wang X, Nesterov V, Venero A F and Omary M A 2011 Fluorous metal–organic frameworks with superior adsorption and hydrophobic properties toward oil spill cleanup and hydrocarbon storage *J. Am. Chem. Soc.* **133** 18094–7
- [122] Kolb B and Thonhauser T 2011 van der Waals density functional study of energetic, structural, and vibrational properties of small water clusters and ice *i<sub>h</sub>* *Phys. Rev. B* **84** 045116
- [123] Skoulidas A I and Sholl D S 2005 Self-diffusion and transport diffusion of light gases in metal–organic framework materials assessed using molecular dynamics simulations *J. Phys. Chem. B* **109** 15760–8
- [124] Haldoupis E, Watanabe T, Nair S and Sholl D S 2012 Quantifying large effects of framework flexibility on diffusion in MOFs: CH<sub>4</sub> and CO<sub>2</sub> in ZIF-8 *ChemPhysChem* **13** 3449–52
- [125] Yang Q and Zhong C 2005 Molecular simulation of adsorption and diffusion of hydrogen in metal–organic frameworks *J. Phys. Chem. B* **109** 11862–4
- [126] Amirjalayer S, Tafipolsky M and Schmid R 2007 Molecular dynamics simulation of benzene diffusion in MOF-5: importance of lattice dynamics *Angew. Chem. Int. Edn* **46** 463–6
- [127] Skoulidas A I 2004 Molecular dynamics simulations of gas diffusion in metal–organic frameworks: argon in cubtc *J. Am. Chem. Soc.* **126** 1356–7
- [128] Haldoupis E, Nair S and Sholl D S 2010 Efficient calculation of diffusion limitations in metal organic framework materials: a tool for identifying materials for kinetic separations *J. Am. Chem. Soc.* **132** 7528–39
- [129] Liu B, Yang Q, Xue C, Zhong C and Smit B 2008 Molecular simulation of hydrogen diffusion in interpenetrated metal–organic frameworks *Phys. Chem. Chem. Phys.* **10** 3244–9
- [130] Queen W L, Brown C M, Britt D K, Zajdel P, Hudson M R and Yaghi O M 2011 Site-specific CO<sub>2</sub> adsorption and zero thermal expansion in an anisotropic pore network *J. Phys. Chem. C* **115** 24915–9
- [131] Bao Z, Yu L, Ren Q, Lu X and Deng S 2011 Adsorption of CO<sub>2</sub> and CH<sub>4</sub> on a magnesium-based metal organic framework *J. Colloid Interface Sci.* **353** 549–56
- [132] Ebrahim A M, Levasseur B and Bandosz T J 2013 Interactions of NO<sub>2</sub> with Zr-based MOF: effects of the size of organic linkers on NO<sub>2</sub> adsorption at ambient conditions *Langmuir* **29** 168–74
- [133] Yu J, Ma Y and Balbuena P B 2012 Evaluation of the impact of H<sub>2</sub>O, O<sub>2</sub>, and SO<sub>2</sub> on postcombustion CO<sub>2</sub> capture in metal–organic frameworks *Langmuir* **28** 8064–71
- [134] Yu K and Schmidt J R 2013 Comment on ‘how well do metal–organic frameworks tolerate flue gas impurities?’ *J. Phys. Chem. C* **117** 3192
- [135] Ding L and Özgür Yazaydin A 2012 How well do metal–organic frameworks tolerate flue gas impurities? *J. Phys. Chem. C* **116** 22987–91
- [136] Coudert F-X, Mellot-Draznieks C, Fuchs A H and Boutin A 2009 Prediction of breathing and gate-opening transitions upon binary mixture adsorption in metal–organic frameworks *J. Am. Chem. Soc.* **131** 11329–31
- [137] Gücüyener C, van den Bergh J, Gascon J and Kapteijn F 2010 Ethane/ethene separation turned on its head: selective ethane adsorption on the metal–organic framework ZIF-7 through a gate-opening mechanism *J. Am. Chem. Soc.* **132** 17704–6
- [138] Pera-Titus M and Farrusseng D 2012 Guest-induced gate opening and breathing phenomena in soft porous crystals: building thermodynamically consistent isotherms *J. Phys. Chem. C* **116** 1638–49